MALAYSIAN JOURNAL OF SCIENCE
MJS
ISSN 1394-3065

Regular Issue

Malaysian Journal of Science 43 (2): 96-103 (June 2024) https://mjs.um.edu.my

SURFACE PLASMON RESONANCE ANALYSIS FOR BENZENE SENSING MEDIA USING SILVER AND Ta_2O_5 THIN FILMS

Haidar J. Mohamad[1a]*, Shaymaa H. Kafi[2a], Farah J. Kadhum[3a]

Abstract: The increasing demand for optical sensors is driven by their wide applications, making surface plasmon resonance (SPR) play a crucial role in this field. In this study, a multilayered thin film consisting of tantalum pentoxide (Ta_2O_5) and silver (Ag) deposited on a glass prism was used to study SPR. The Ag layer thickness was fixed at 50 nm, while the Ta_2O_5 layer thickness varied from 0 to 70 nm. The Kretschmann configuration was employed to assess the sensitivity of air and gases with different refractive indices. Therefore, different layer thicknesses along with different wavelengths and angles were investigated. MATLAB software was employed to simulate and analyze SPR with a half-sphere prism to extend the incident angle. The simulation conditions with Fresnel equations were used to calculate the reflectivity and transmittance coefficients for the studied sample. The results revealed that the best output was at a Ta_2O_5 thickness of 50 nm to get optimal full width at half maximum of 2.4 and sensitivity factor of 162.5. This device works in the visible and infrared regions.

Keywords: *Thin film, modeling, optical sensor, sensor sensitivity.*

1. Introduction

Tantalum pentoxide (Ta_2O_5) thin films have remarkable properties, including a high dielectric constant. In the visible region, these films have a high refractive index as well as high transmittance and high-temperature resistance [1]. Surface plasmon resonance (SPR), used for sensor applications, has emerged as a branch of modern technology. It has a fast response, can work with small-volume materials, and is highly sensitive to changes in the refractive index of the medium located near the thin metal film. SPR-based sensors are used extensively in optical devices and sensing applications, including biomolecular detection [2], medical diagnosis [3], biological analyses [4], antibody–antigen interaction [5], organic chemical sensing [6], bioimaging [7], environmental safety [8], and water testing [9]. It has been employed in optoelectronic devices, such as SPR imaging and film thickness monitoring [10].

All materials interact with light in a certain manner. This interaction of photons with a crystal or electronic structure of matter leads to several phenomena, such as reflection, refraction, transmission, and absorption [11]. The value of reflectivity depends on the angle of incidence. Materials with a higher refractive index have a higher reflectivity than those with a lower refractive index [12]. The optical properties of a material are related to its interaction with electromagnetic radiation. Generally, plasmonic devices require metallic components with an abundance of free electrons. Free electrons display negative permittivity, which is considered an essential property of any plasmonic material. These electrons are affected by any electromagnetic wave, resulting in oscillation and the surface plasmon phenomenon [13].

SPR sensor devices have a complex optical system design and may have expensive components [14]. Therefore, simulation analytics are crucial in constructing SPR sensors, optimizing optical parameters, and reducing operational costs [15]. Several studies concentrated on simulations to demonstrate the advantages and disadvantages of SPR. Wen *et al.* (2020) presented the kinetics of the plasmon model and explained how they depended on the particle simulation method. The modeling of a single electron in plasmon excitation included two steps to locate electron movement and reveal electron spill-out effects [16]. However, they did not explore this field altogether, leaving room for further investigation.

Costa et al. (2019) analyzed multilayer reflectance using Otto's configuration. The incident light angle range starts from 30° to 40°, which is small compared with our work [17]. Hassan et al. (2020) proposed a photonic crystal fiber sensor whose output analysis depends on its refractive index. They performed simulations using the finite element method. They suggested a design with airholes in hexagonal shapes, and the center airhole was benzene coated with gold to generate the plasmon effect. The high performance was in the refractive index from 1.45 to 1.49 only [18]. Kumar et al. (2021) investigated the hybrid structure of BP–Ti3C2Tx with Cu–Ni layers for biochemical sensor applications. They noticed that by changing the thickness of the Cu–Ni layers, the sensitivity was enhanced and could be optimized [18]. Farah et al. (2021) simulated multilayer samples of Au–Si3N4 at different thicknesses deposited on the N-LASF9 glass. They studied different wavelengths and incident angles to

Authors information:
[a]Mustansiriyah University - College of Science- Physics Dept., Baghdad, IRAQ. Email: haidar.mohamad@uomustansiriyah.edu.iq[1]; iraqshaymaa.h.kafy@uomustansiriyah.edu.iq[2]; farahjawadalnuaimi@uomustansiriyah.edu.iq[3]
*Corresponding Author: haidar.mohamad@uomustansiriyah.edu.iq

Received: February 17, 2023
Accepted: May 31, 2023
Published: June 30, 2024

DOI:https//doi.org/10.22452/mjs.vol43no2.10
Malaysian Journal of Science 43(2): 96-103(June 2024)

plot the resonance angle of SPR with reflection. The sensor had a range of 600–700 nm and 900–1000 nm [19].

In this study, the primary reason behind using silver/tantalum pentoxide (Ag/ $Ta_2O_5$is to modify the absorption capacity of incident light and enhance the interface effect between layers. An SPR system was simulated to detect the benzene medium. This system consists of a Ta2O5 layer used as a waveguide medium and a silver (Ag) layer deposited on the glass prism in the Kretschmann configuration. The behavior of the SPR curve was examined by changing the sample thickness and the incident angle for different wavelengths. It gives the sensing range of wavelengths and optimal angles to attain resonant surface plasmon.

2. Methodology

When light interferes with a medium, the electrons oscillate harmonically with the incident light. In the case of SPR, oscillation and propagation occur along the interface between the dielectric and metal mediums. SPR depends on observing the reflected light spectrum obtained by angular or wavelength interrogation [20]. Therefore, the angular change resolution is preferred when investigating SPR. Measuring the change in resonant angle allows the extraction from the spectrum the reflectance curve as a function of incident angle for the same wavelength. This spectrum gives two significant factors to describe the SPR curve: minimum reflectance and full width at half maximum (FWHM). Noble metals such as Au and Ag have been used to propagate polarizing waves in surface plasma at a specific wavelength [21].

The Kretschmann configuration was used in the simulation of the SPR sensor system in this work (Figure 1). The sensor consists of a LaSF9 glass prism, Ag thin film with a thickness of 50 nm, a Ta2O5 layer of varying thicknesses (d = 0, 25, 50, and 75 nm), and a sensing medium considered to be benzene (C6H6) with the refractive index changed by Δn = 0 and 0.04.

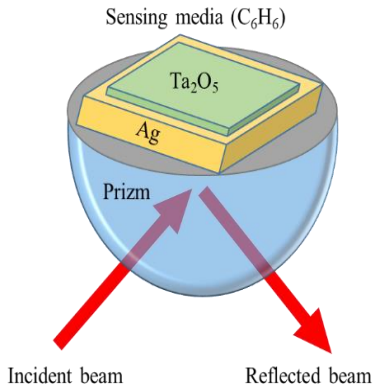

Figure 1. The schematic diagram of the SPR system based on the Kretschmann configuration.

The complex refractive index (nm) can be calculated due to the reaction of light with the semi-transparent matter as follows [22]:

$$n_m = n_r + in_k \quad (1)$$

Where n_r represents the real part of the refractive index. The imaginary part, n_k, is called the extinction coefficient, which also refers to the amount of attenuation coefficient along the z-direction. The complex refractive index (n) is related to the wave number (k) by k = 2πn/λ. The electromagnetic wave plane component for any wavelength in the vacuum can be expressed as follows [22]:

$$E_{(z,t)} = E_o e^{i(kz-wt)} = E_o e^{\frac{i(2\pi(n_r+in_k)z}{\lambda}-wt)} = e^{\frac{-2\pi n_k z}{\lambda}}\left[E_o e^{i\left(\frac{2\pi n_r z}{\lambda}-wt\right)}\right] n_m = n_r + in_k \quad (2)$$

The electromagnetic wave exponentially decays with (z) by the factor $e^{-\left(\frac{2\pi n_k z}{\lambda}\right)}$; thus, the attenuation coefficient becomes $\alpha = \frac{4\pi k}{\lambda}$. n_r and nk are frequency dependent, and nk has two conditions, namely, nk > 0 and nk = 0, meaning that the light is absorbed by media and travels without loss, respectively.

Dielectrics have greater absorption capacity compared with metals. Dielectric-like glass has very low DC conductivity and negligible loss at low frequencies, leading to small absorption values. Although the absorption increases dramatically at high frequencies, it can be reduced by the transparent material properties. The Kramers–Kronig relations determine the complex refractive index of real and imaginary components, nr and nk, respectively. These components are measured indirectly by calculating the reflectance and transmittance of the sample [23].

Ag is considered one of the most favorable materials used as a sensing metal because of its high electric field conductivity and low imaginary component of its refractive index [24]. Ta2O5 also has favorable properties such as a high refractive index (2.05–2.30) within the visible band, a large energy gap of 4.2 eV, and no absorption within the range of 10 to 400 nm [25]. Therefore, it is necessary to plot the behavior of the refractive index as a function of wavelength for all the substrates (glass prism), an Ag layer, Ta2O5, and C6H6. The data in Figure 2 were collected online [26].

DOI:https//doi.org/10.22452/mjs.vol43no2.10
Malaysian Journal of Science 43(2): 96-103(June 2024)

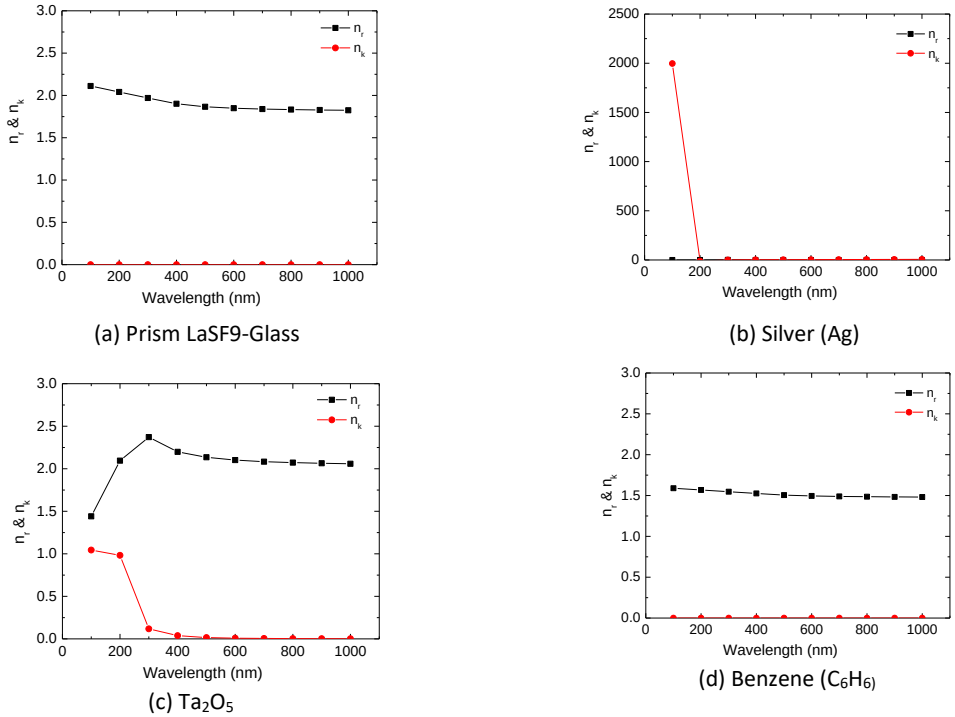

(a) Prism LaSF9-Glass (b) Silver (Ag)

(c) Ta_2O_5 (d) Benzene (C_6H_6)

Figure 2. Real (n) and Imaginary (k) parts the with the wavelength (λ) for (a) prism, (b) Ag layer, (c) Ta2O5, and (d) C6H6.

The change in the refractive index due to the interaction between light and the sample's surface led to the shift in the SPR curve. Therefore, the details of the SPR curve are significant as the indicator for the sensing tool [27]. We used the Kretschmann configuration for the studied sample to understand the SPR curve. The reflectivity of the multilayer sample is presented by Fresnel's equations: the first layer boundary (Ea and Ha) and the last layer boundary (EN and HN) for the electric and magnetic field component amplitudes, respectively. It can be represented by the total matrix [28]:

$$[\,E_a\ H_{\,a}\,] = \left[\prod_{m=1}^{N} M_m\right][\,E_N\ H_{\,N}\,] = [M_{11}\ M_{12}\ \ M_{21}\ M_{22}\ ][E_N\ \ H_N\ ] \tag{3}$$

The transfer matrix method was used to investigate the optical properties of the suggested SPR sensor. The light interaction matrix M_m of the mth layer (m = 1 to N) can be expressed by [29]:

$$M_m = \begin{bmatrix} cos\ cos\ \beta_m & \dfrac{i}{q_m} \\ sin\ sin\ \beta_m & iq_m sin\ \beta_m \qquad cos\ \beta_m \end{bmatrix} \tag{4}$$

Where β_m and q_m are defined as $\left(\frac{2\pi}{\lambda}\right) n_m d_m\ cos\ cos\ \theta_m$ and $n_m\ cos\ cos\ \theta_m$, respectively. n_m is the complex refractive index, θ_m is the incidence angle of mth layer. This equation is important to model the electric and magnetic component field interfaced of mth layer.

The description of the single field that passes through layer m can be given by

$$\beta_m = \left(\frac{2\pi}{\lambda}\right) n_m d_m\ cos\ cos\ \theta_m \tag{5}$$

The p-polarization field for any layer (q_m) is represented by [30]:

$$q_m = \frac{n_m\sqrt{\varepsilon_o \mu_o}}{cos\ cos\ \theta_m} \tag{6}$$

where $\varepsilon_o\ and\ \mu_o$ are the vacuum permittivity and the permeability, respectively.

From the preceding matrix, Fresnel's reflection coefficient (r) and transmission coefficient (t) within the sample are obtained as follows [29]:

$$r = \frac{[q_N M_{11} + q_o q_N M_{12}] - [M_{21} + q_o M_{22}]}{[q_N M_{11} + q_o q_N M_{12}] + [M_{21} + q_N M_{22}]} \tag{7}$$

$$t = \frac{2q_o\left(\frac{n_N}{n_o}\right)}{[q_N M_{11} + q_o q_N M_{12}] + [M_{21} + q_N M_{22}]} \tag{8}$$

DOI:https//doi.org/10.22452/mjs.vol43no2.10
Malaysian Journal of Science 43(2): 96-103(June 2024)

The total reflectance (R) and the total transmittance (T) are given by [29]:

$$R = |r|^2 \quad (9)$$

$$T = |t|^2 \quad (10)$$

The most significant parameter of any SPR sensor is its sensitivity. Sensitivity can be explained in terms of the marked change in the resonance angle ($\Delta\theta_{SPR}$). This change is caused by the changes in the refractive index (n_m) of the sensing medium. Therefore, the parameters of the sensing medium are vital, for instance, sample thickness, number of layers, material specifications, and shape or design. The sensitivity equation is written as [31]:

$$S = \left(\frac{\Delta\theta_{SPR}}{\Delta n}\right) \quad (11)$$

where $\Delta\theta_{SPR}$ is the resonance angle change, Δn_m is the change in the refractive index. $\Delta\theta_{SPR}$ is related to the minimum reflectance (R_{min}) and its value is extracted from the R–θ curve.

In terms of sensing performance, the resonance is dependent on the Ta2O5 layer thickness. In this study, the performance characteristics of the noble metal Ag/dielectric Ta2O5 sensor were studied by carefully carrying out a sophisticated MATLAB algorithm of SPR simulation followed by determining SPR curve characteristics. Reflectance (R) was simulated as a function of the incident angle for the Ag/Ta2O5 structure. Ag thickness was fixed at 50 nm, whereas the thickness of the dielectric slab Ta2O5 was varied (d = 0, 25, 50, and 75 nm). Here, the dielectric Ta2O5 acts as a waveguide medium, supporting the propagation of waveguide modes within the selected sample.

The simulation of the experimental data was achieved using the following algorithm:

Compute FWMH and L_d algorithm

The dip data are represented by y=f(x), where x represents the incident angle (0° to 90°).

Start algorithm

1. Extract maximum SPR peak curve (L_d) at SPR angle (SPR_Theta) using [Ld SPR_Theta]=min(y)
2. Extract the half max value for the SPR peak curve: **halfMax** = (min(y) + max(y)) / 2;
3. Extract data at curve decay below **halfMax** value and save it in *halfmax1*.
4. Extract data at curve above **halfMax** value and save it in *halfmax2*.
5. Compute FWHM using FWMH = halfmax2- halfmax1

End algorithm

DOI:https//doi.org/10.22452/mjs.vol43no2.10
Malaysian Journal of Science 43(2): 96-103(June 2024)

3. Results and Discussion

In this study, we investigated the direct effect of the change in Ta2O5 layer thickness on the sensitivity of the suggested SPR sensor. Therefore, the Ag layer thickness was precisely fixed at 50 nm, while the Ta2O5 layer thickness was varied from 0 to 70 nm. Figure 3 depicts the reflectance curves as a function of light incident angles (θ) for a different Ta2O5 layer thickness and different wavelengths (λ) from 100 to 1000 nm, with a step size of 100 nm.

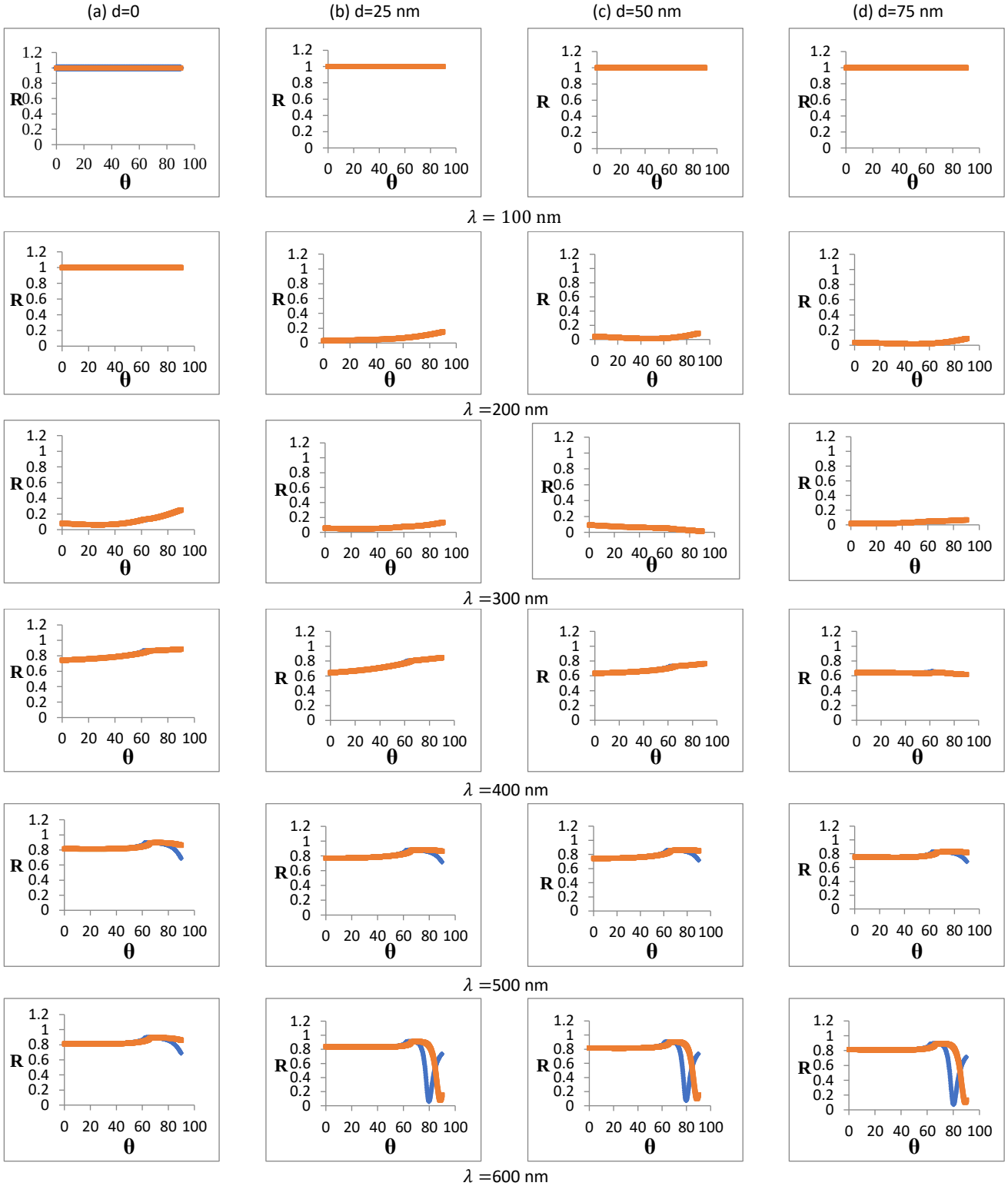

DOI:https//doi.org/10.22452/mjs.vol43no2.10
Malaysian Journal of Science 43(2): 96-103(June 2024)

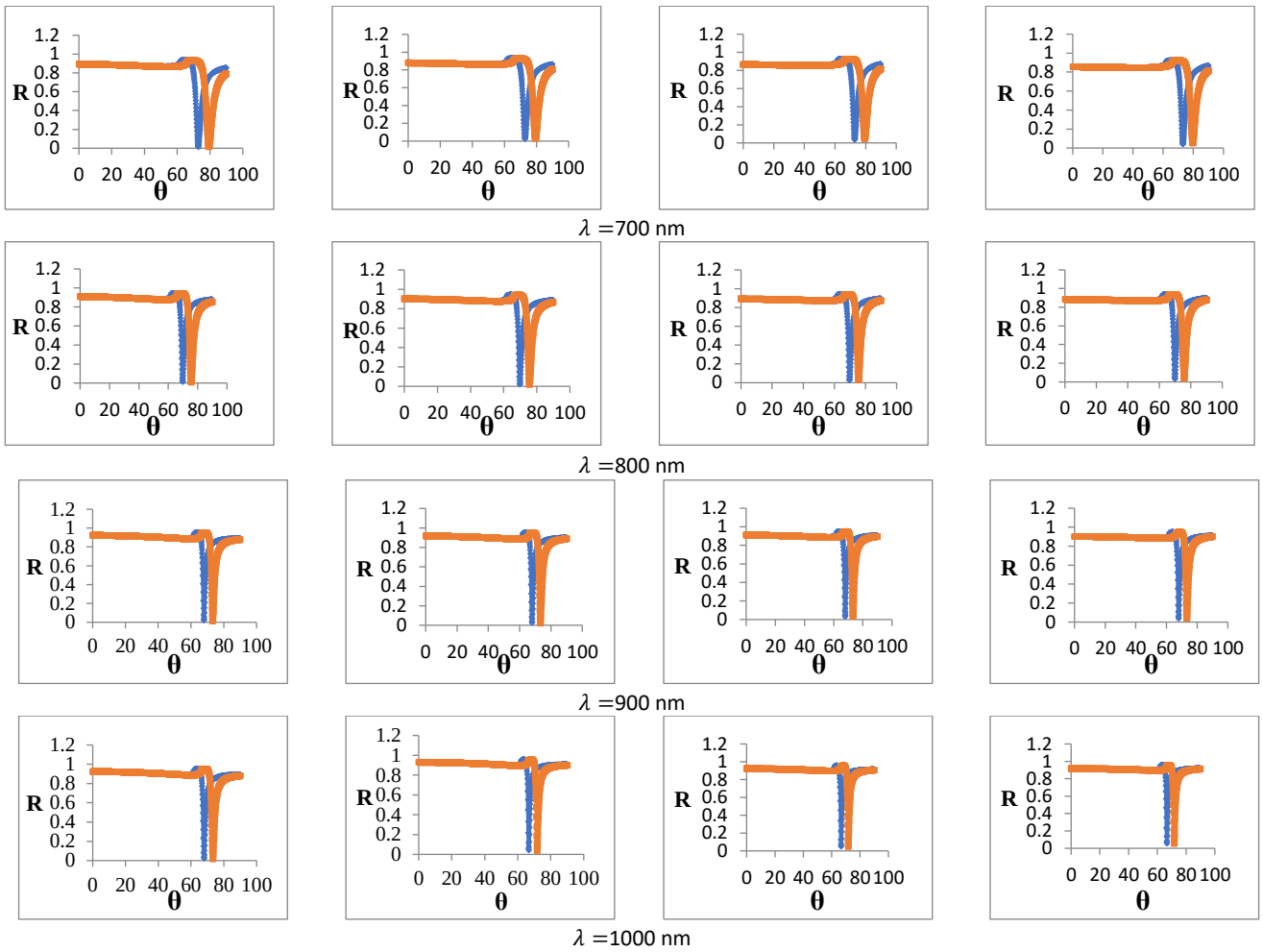

Figure 3. Reflectance of the suggested sample with incidence light angle for different wavelengths (λ=100-1000 nm) and different Ta_2O_5 layer thicknesses (a) d=0 nm, (b) d=25 nm, (c) d=50 nm, and (d) d=75 nm. The blue line is $\Delta n_m = 0$, and red line $\Delta n_m = 0.04$

Figure 3 demonstrates that there is no effect of resonance from wavelength 100 to 600 nm, and the effect becomes discernible at wavelength 700 nm. Evidently, the shift between the blue and red curves, caused by the change in the refractive index, is significant for SPR sensor performance. The shape of the dip, like its width and height, is also significant.

The results of R–θ curve analysis data are presented in Tables 1–4, showing FWHM, dip length (Ld), and S values with change in the refractive index of C6H6 (Δn_m) with d = 0 to 75 nm. The numerical results of Ag–Pt bimetallic films were used to simulate the SPR within a small range due to the prism diagram [32]. They show that the FWHM changed with the layer thickness. Our system works with a wide range of angles and is sensitive to the visible and IR range, which offers a wide range of applications.

Table 1. Data corresponding to wavelengths 700–1000 nm at thickness 0.

λ(*nm*)	Δ*n*	θ_{SPR}	FWHM	L_d	S
700	0	72.9	3.7	0.9191	160.0
	0.04	79.3	4.6	0.9169	
800	0	69.8	2.5	0.9321	142.5
	0.04	75.5	3.0	0.9325	
900	0	76.9	1.7	0.9329	132.0
	0.04	73.2	2.1	0.9350	
1000	0	66.7	1.3	0.9214	125.0
	0.04	71.7	1.6	0.9260	

Table 2. Data corresponding to wavelengths 700–1000 nm of the R–θ curve at thickness 25 nm.

λ(*nm*)	Δ*n*	θ_{SPR}	FWHM	L_d	S
700	0	72.9	3.5	0.9044	160.0
	0.04	79.3	4.4	0.8983	
800	0	69.8	2.4	0.9233	142.5
	0.04	75.5	2.9	0.9220	
900	0	67.9	1.6	0.9257	132.0
	0.04	73.2	2.0	0.9262	
1000	0	66.7	1.2	0.9144	125.0
	0.04	71.7	1.5	0.9181	

DOI:https//doi.org/10.22452/mjs.vol43no2.10
Malaysian Journal of Science 43(2): 96-103(June 2024)

Table 3. Data corresponding to wavelengths 700–1000 nm of the R–θ curve at thickness 50 nm

λ(*nm*)	Δ*n*	θ_{SPR}	FWHM	L_d	S
700	0	69.9	2.4	0.9138	162.5
	0.04	75.6	2.9	0.9104	
800	0	69.8	2.4	0.9233	142.5
	0.04	75.5	2.9	0.9220	
900	0	67.9	1.6	0.9175	132.5
	0.04	73.2	2.0	0.9163	
1000	0	66.7	1.2	0.9068	125.0
	0.04	71.7	1.5	0.9086	

Table 4. Data corresponding to wavelengths 700–1000 nm of the R–θ curve at thickness 75 nm.

λ(*nm*)	Δ*n*	θ_{SPR}	FWHM	L_d	S
700	0	73.0	3.5	0.8803	162.5
	0.04	79.5	4.4	0.8685	
800	0	69.9	2.3	0.9067	142.5
	0.04	75.6	2.8	0.9011	
900	0	67.9	1.6	0.9097	132.5
	0.04	73.2	2.0	0.9068	
1000	0	66.7	1.2	0.8997	125.0
	0.04	71.7	1.5	0.8989	

The summary Figure 3 shows that SPR does not appear at wavelengths from 100 to 500 nm. SPR begins to appear at the wavelength of 600 nm and has an incomplete dip. At wavelengths 700, 800, 900, and 1000 nm, SPR appears at all oxide layer thicknesses. The minimum reflectivity (Rmin) in the R–θ curve is 0.061. This value was recorded at wavelength 900 nm with θSPR= 73.2°. The sensor resolution changed as the wavelength varied, causing a broadening of the reflectance dip. The shape dip and its width determine the accuracy of the sensor. The highest dip length is (0.935°) at λ = 900 nm and thickness d = 25 nm. The higher sensitivity (S) for the proposed SPR sensor obtained with sharper shapes is 162.5.

The FWHM plays a critical role because the resonance angle in the R–θ curve should be small to be distinguished with small changes compared with different wavelengths. The sharper and narrower dip shape of SPR and the smaller value of FWHM result in high detection accuracy. Furthermore, it is worth noting that when Ld value approaches 1, a good SPR is achieved. Therefore, controlling the sample thickness is vital to get a low FWHM value and a Ld value approaching 1. The presented algorithm gives accurate details to calculate FWHM, and equation 5 gives the value of the sensitivity of the suggested sensor.

4. Conclusions

The suggested sample for the optical sensor has many positive and important points. The sensitivity (S) increases significantly with the appearance of the Ta_2O_5 layer because it works as a waveguide and increases the resonance signal. The relationship between the change in the Ta_2O_5 layer thickness and the refractive index of the sensing medium has a minor influence. The R–θ curve dip shifted in this case due to the changes in the refractive index. Therefore, the SPR dip width should be smaller to distinguish the small shift at Δn reaching zero. The suggested SPR sensor detects a small variation in the refractive index (0.04) of the proposed sensing medium. The suggested device works in the visible and IR regions of the electromagnetic spectrum, as shown in the R–θ curve. It is important to increase the step size in modeling to get the behavior of the resonance dip because it is sensitive to a small angle value.

5. Acknowledgement

The authors would like to thank the Department of Physics/College of Science/Mustansiriyah University (www.uomustansiriyah.edu.iq) in Baghdad, Iraq, for their support in the present work.

6. References

Abdul-Hussain, M. A., and Mohamad, H. J. (2021). "Thermal Effect in a 3-D Simulation within Multilayer Thin Film of Ultrafast-Pulsed Laser". Al-Mustansiriyah Journal of Science, 32(4), 104-109; : http://doi.org/10.23851/mjs.v32i4.1039

Abdul-Hussain, M. A., Mohamad, H. J., and Al-Haddad, A. (2022). "1-D Simulation of Ultrafast-Pulsed Laser into Nano-Sized Multilayered Structure (Ni81Fe19/Cu/YIG/GGG) for Memory Device Applications". Iraqi Journal of Science, 63(3), 1045-1054; https://doi.org/10.24996/ijs.2022.63.3.14

Ali, M. Z. (2021). "Plasmon-polariton gap and associated phenomenon of optical bistability in photonic hypercrystals". Physics Letters A, 387(n/a), 127026; https://doi.org/10.1016/j.physleta.2020.127026

Alias, R., Mahmoodian, R., and Abd Shukor, M. H. (2019). "Development and characterization of a multilayer silver/silver-tantalum oxide thin film coating on stainless steel for biomedical applications". International Journal of Adhesion and Adhesives, 92(n/a), 89-98; https://doi.org/10.1016/j.ijadhadh.2019.04.010

Anand, U., Chandel, A. K. S., Oleksak, P., Mishra, A., Krejcar, O., Raval, I. H., and Kuca, K. (2022). "Recent advances in the potential applications of luminescence-based, SPR-based, and carbon-based biosensors". Applied Microbiology and Biotechnology, 106(8), 2827-2853; https://doi.org/10.1007/s00253-022-11901-6

Balaur, E., Sadatnajafi, C., and Abbey, B. (2022); "Optical barcoding using polarisation sensitive plasmonic biosensors for the detection of self-assembled monolayers". Scientific Reports, 12(1), 13081; : https://doi.org/10.21203/rs.3.rs-1360592/v1

Bereli, N., Bakhshpour, M., Topçu, A. A., and Denizli, A. (2021). "Surface Plasmon Resonance-Based Immunosensor for Igm Detection with Gold Nanoparticles. Micromachines", 12(9), 1092; https://doi.org/10.3390/mi12091092

Berguiga, L., Ferrier, L., Jamois, C., Benyattou, T., Letartre, X., and Cueff, S. (2021). Ultimate phase sensitivity in surface plasmon resonance sensors by tuning critical coupling with phase change materials. Optics Express, 29(25), 42162-42175; https://doi.org/10.1364/OE.439869

DOI:https//doi.org/10.22452/mjs.vol43no2.10
Malaysian Journal of Science 43(2): 96-103(June 2024)

Böer, K. W., and Pohl, U. W. (2018). "Interaction of Light with Solids". In K. W. Böer and U. W. Pohl (Reds.), Semiconductor Physics (pp. 333-388). Cham: Springer International Publishing. https://link.springer.com/referenceworkentry/10.1007/978-3-319-69150-3_10

Costa, E. B., Rodrigues, E. P., and Pereira, H. A. (2019). "Sim-SPR: an Open-Source Surface Plasmon Resonance Simulator for Academic and Industrial Purposes". Plasmonics, 14(6), 1699-1709, https://doi.org/10.1007/s11468-019-00970-5

Ding, Wen J., Lim, Jeremy Zhen J., Do Hue Thi Bich, Xiong Xiao, Mahfoud Zackaria, Png Ching Eng, Bosman Michel, Ang Lay Kee, and Wu Lin (2020). "Particle simulation of plasmons". Nanophotonics 9(10), 3303-3313; https://doi.org/10.1515/nanoph-2020-0067

Ding, Wen J., Lim, Jeremy Zhen J., Do Hue Thi Bich, Xiong Xiao, Mahfoud Zackaria, Png Ching Eng, Bosman Michel, Ang Lay Kee, and Wu Lin (2020). "Particle simulation of plasmons". Nanophotonics 9(10), 3303-3313; https://doi.org/10.1515/nanoph-2020-0067

Divya, J., Selvendran, S., Raja, A. S., and Sivasubramanian, A. (2022). "Surface plasmon based plasmonic sensors: A review on their past, present and future". Biosensors and Bioelectronics: X, 11(n/a), 100175; https://doi.org/10.1016/j.biosx.2022.100175

Duan, Q., Liu, Y., Chang, S., Chen, H., and Chen, J.H. (2021). "Surface Plasmonic Sensors: Sensing Mechanism and Recent Applications". Sensors (Basel, Switzerland), 21(16), 5262; https://doi.org/10.3390/s21165262

Farah, J. K., Shaymaa, H. K., Asrar, A. S., Ali, A. D. Z., and Anwar, H. S. (2021). "Simulation of Surface Plasmon Resonance (SPR) of Silver with Titanium Oxide as a BiLayer Biosensor". The Scientific Journal of King Faisal University, 22(2), (n/a); https://doi.org/10.37575/b/sci/210046

Ferrari, J. L., Lima, K. d. O., and Gonçalves, R. R. (2021). "Refractive Indexes and Spectroscopic Properties to Design Er3+-Doped SiO2–Ta2O5 Films as Multifunctional Planar Waveguide Platforms for Optical Sensors and Amplifiers". ACS Omega, 6(13), 8784-8796; https://doi.org/10.1021/acsomega.0c05351

Harumi, A., Endo, K., and Suzuki, T. (2021). "Reflectionless metasurface with high refractive index in the terahertz waveband". Optics Express, 29(10), 14513-14524; https://doi.org/10.1364/OE.420827

Kumar, R., Pal, S., Pal, N., Mishra, V., and Prajapati, Y. K. (2021). "High-performance bimetallic surface plasmon resonance biochemical sensor using a black phosphorus–MXene hybrid structure". Applied Physics A, 127(n/a), 1-12; https://doi.org/10.1007/s00339-021-04408-w

Lee, H.T., Ji, G.S., Oh, J.Y., Seo, C.W., Kang, B.W., Kim, K.W., and Park, H.R. (2021). "Measuring Complex Refractive Indices of a Nanometer-Thick Superconducting Film Using Terahertz Time-Domain Spectroscopy with a 10 Femtoseconds Pulse Laser. Crystals, 11(6), 651; https://doi.org/10.3390/cryst11060651

Li, J., Han, D., Zeng, J., Deng, J., Hu, N., and Yang, J. (2020). "Multi-channel surface plasmon resonance biosensor using prism-based wavelength interrogation". Optics Express, 28(9), 14007-14017; https://doi.org/10.1364/OE.389226

Mishra, S. K., Verma, R. K., and Mishra, A. K. (2021). "Versatile Sensing Structure: GaP/Au/Graphene/Silicon". Photonics, 8(12), 547. https://doi.org/10.3390/photonics8120547

Mohamad, H. J., Shelford, L. R., Aziz, M., Al-Jarah, U. A. S., Al-Saigh, R., Valkass, R. A. J., and Hicken, R. J. (2017). "Thermally induced magnetization dynamics of optically excited YIG\Cu\Ni81Fe19 trilayers". Physical Review B, 96(13), 134431; https://doi.org/10.1103/PhysRevB.96.134431

Mulyanti, B., Nugroho, H. S., Wulandari, C., Rahmawati, Y., Hasanah, L., Hamidah, I., and Majlis, B. Y. (2022). "SPR-Based Sensor for the Early Detection or Monitoring of Kidney Problems". International Journal of Biomaterials, 2022(n/a), 9135172; https://doi.org/10.1155/2022/9135172

Pandaram, M., Santhanakumar, S., Veeran, R., Balasundaram, R. K., Jha, R., and Jaroszewicz, Z. (2022). "Platinum Layers Sandwiched Between Black Phosphorous and Graphene for Enhanced SPR Sensor Performance". Plasmonics, 17(1), 213-222; https://doi.org/10.1007/s11468-021-01507-5

Polyanskiy, M. N. (2022). Refractive index database. van https://refractiveindex.info

Prosposito, P., Burratti, L., and Venditti, I. (2020). "Silver Nanoparticles as Colorimetric Sensors for Water Pollutants". Chemosensors, 8(2), 26; https://doi.org/10.3390/chemosensors8020026

Sai, T., Saba, M., Dufresne, E. R., Steiner, U., and Wilts, B. D. (2020). "Designing refractive index fluids using the Kramers–Kronig relations". Faraday Discussions, 223(0), 136-144; 10.1039/D0FD00027B

Shpacovitch, V., and Hergenröder, R. (2020). "Surface Plasmon Resonance (SPR)-Based Biosensors as Instruments with High Versatility and Sensitivity". Sensors (Basel, Switzerland), 20(11), 3010; https://doi.org/10.3390/s20113010

Singh, G. P., and Sardana, N. (2022). "Smartphone-based Surface Plasmon Resonance Sensors: a Review". Plasmonics, 17 (n/a), 1869–1888; https://doi.org/10.1007/s11468-022-01672-1

Steglich, P., Giulia, L., and Andreas, M. (2022). "Surface Plasmon Resonance (SPR) Spectroscopy and Photonic Integrated Circuit (PIC) Biosensors: A Comparative Review". Sensors, 22(8). doi:10.3390/s22082901; https://doi.org/10.3390/s22082901

Uddin, S. M. A., Chowdhury, S. S., and Kabir, E. (2021). "Numerical Analysis of a Highly Sensitive Surface Plasmon Resonance Sensor for SARS-CoV-2 Detection". Plasmonics, 16(6), 2025-2037; https://doi.org/10.1007/s11468-021-01455-0

Wang, X., Deng, H., and Yuan, L. (2021). "Highly Sensitive Flexible Surface Plasmon Resonance Sensor Based on Side-Polishing Helical-Core Fiber: Theoretical Analysis and Experimental Demonstration". Advanced Photonics Research, 2(2), 2000054; https://doi.org/10.1002/adpr.202000054

DOI:https//doi.org/10.22452/mjs.vol43no2.10
Malaysian Journal of Science 43(2): 96-103(June 2024)